Supplemental Information

Anomalous electron transport in epitaxial $NdNiO_3$ films

RHEED: The growth was monitored by in-situ RHEED (reflection high energy electron diffraction). Fig. S1(a) shows the time dependence of intensity of specular reflection (0,0), recorded during the growth of $NdNiO_3$ (NNO) film on $NdGaO_3$ (NGO) substrate and layer-by-layer growth has been confirmed by the sharp drops during ablation and gradual recovery within next few seconds to the same level of intensity after the deposition of each unit cell. Inset of Fig. S1(b) shows RHEED pattern for the NNO film, recorded after cooling to room temperature. The streak patterns of specular and off-specular: (0 1), (0 -1) reflections (in pseudo cubic (p.c.) notation) confirm the desired two-dimensional surface morphology.

X-ray diffraction: Success of epitaxial growth along $[0\ 0\ 1]_{\mathrm{p.c.}}$ has been further confirmed by 2θ-ω scan in X-ray diffraction (Fig. S1(b)). Each diffraction pattern consists of a sharp substrate peak, a broad film peak (indicated by solid triangle in Fig. S1(b)) and thickness fringes, arises due to the finite thickness of film. Out-of plane lattice constant ($c_{\mathrm{p.c.}}$ of NNO films are found to be 3.75 Å (STO), 3.78 Å (NGO), 3.83 Å (SPGO), 3.84 Å (SLAO) and 3.86Å (YAO) and these follow the expected tetragonal distortion relation for the cube on cube growth.

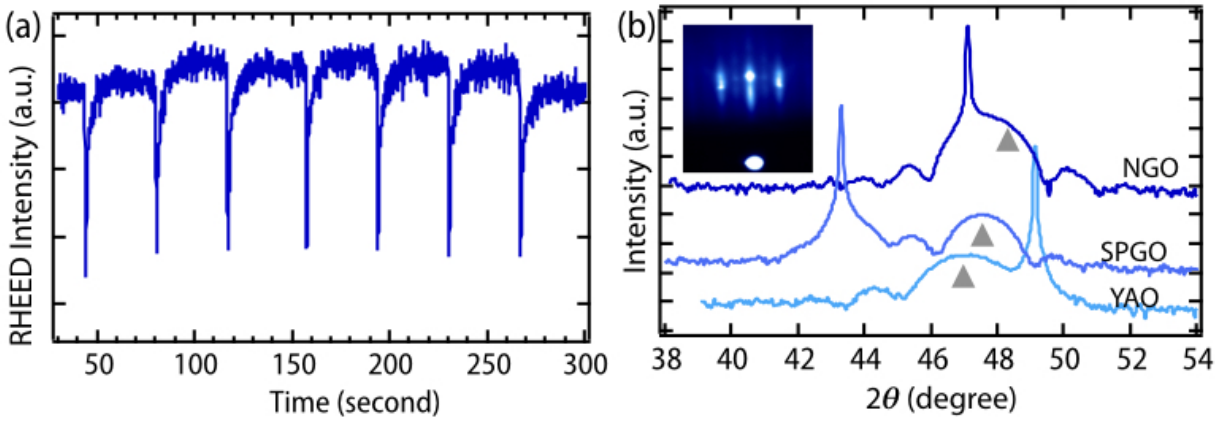

FIG. S1. (a) RHEED specular intensity during the growth of NNO on NGO substrate. (b) The inset shows RHEED pattern of NNO film on NGO substrate, recorded after cooling to room temperature. Representative XRD patterns for NNO films are shown in main panel of (b). The film peaks are marked by △. The sharp peak corresponds to the $(0\ 0\ 2)_{\mathrm{p.c.}}$ reflection for orthorhombic NGO, YAO substrates and (0 0 6) peak for tetragonal SPGO substrate.

Behavior of R_{xy} as a function of magnetic field:

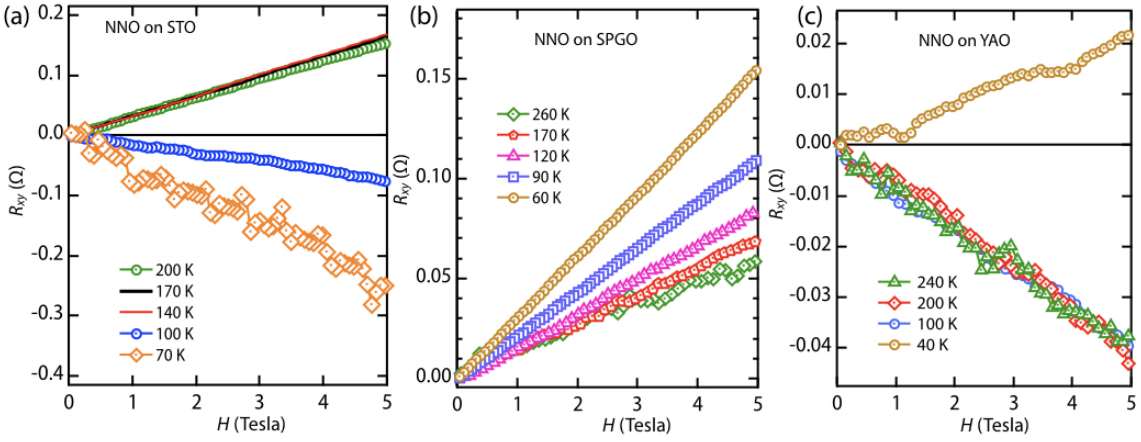

FIG. S2. R_{xy} vs. H after correction for NNO on (a) STO, (b) SPGO and (c) YAO substrate.

Temperature dependence of resistivity:

According to the Fermi liquid theory, the resistivity of a metal behaves as $\rho_{xx} = \rho_0 + AT^n$ with n=2 where ρ_0 represents residual resistivity and A represents the strength of electron-electron scattering. n <2 represents non-Fermi liquid (NFL) behavior. In order to find out the behavior of resistivity in metallic phase of these NNO films, ln($d\rho_{xx}/dT$) vs. ln(T) has been plotted [slope is equal to (n-1)]. This analysis gives a value of n=1.08 (very close to linear behavior) in 180 K-300 K and 130 K-290 K range for NNO on STO (Fig. S3(a)) and SPGO (Fig. S3(b)) respectively. Similar analysis has found n=1.30 (close to NFL characteristic exponent of 4/3) in the interval 10 K-190 K for NNO on YAO and It switches to n=1 in 195 K-290 K range. Similar set of exponent has been also found for NNO film on SLAO substrate.

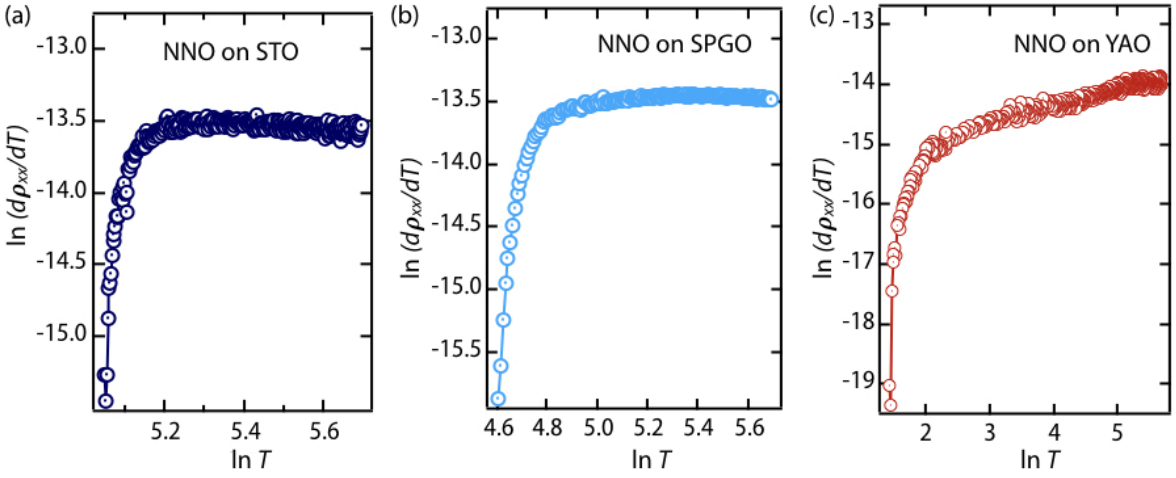

FIG. S3. ln($d\rho_{xx}/dT$) vs. ln(T) for NNO on (a) STO, (b) SPGO, (c) YAO.

Evaluation of carrier concentration: To evaluate the relative carrier concentration among the samples using the equation $R_H = (n_p\mu_p^2 - n_e\mu_e^2)/[e(n_p\mu_p + n_e\mu_e)^2]$, we can further assume (i) $\mu_p = \mu_e$ as both the electron and hole have e_g character and R_H is nearly independent of T, (ii) $n_p + n_e$ is temperature independent and equal to 1 electron per Ni (t_{2g}^6, e_g^1) [1]. Carrier densities n_p and n_e obtained from such analysis (Fig. S4) show a systematic increase and decrease, respectively, with the lowering of epitaxial strain.

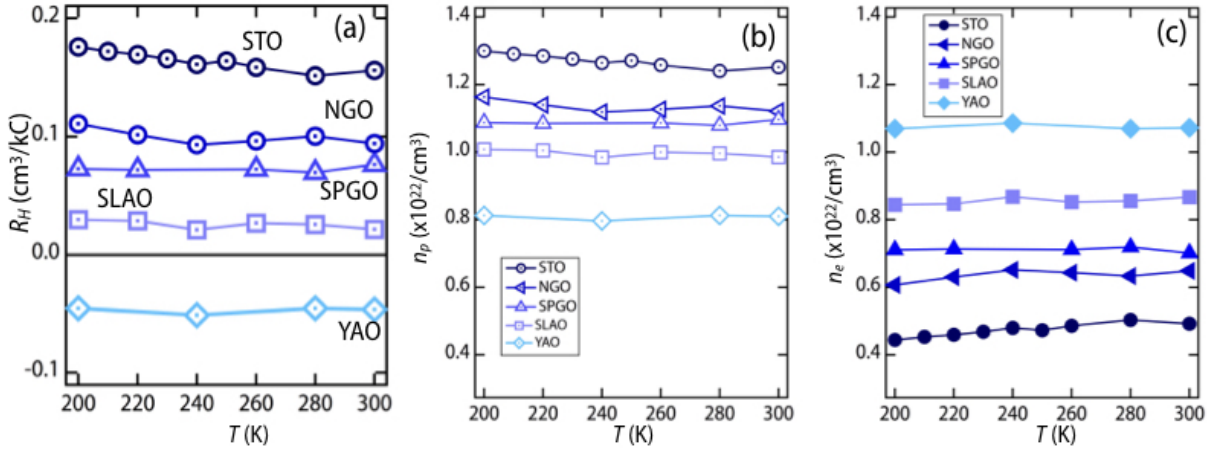

FIG. S4. Temperature dependence of (a) Hall coefficient, (b) hole densities and (c) electron densities for NNO films under different epitaxial strain.

MRDF method

Using the DFT band structures we calculate the electron-electron correlation via the momentum resolved density fluctuation (MRDF) theory [2–5] which includes momentum dependent self-energy effect due to density-density correlations. The MRDF

method is outlined below. We construct the non-interacting Green's function as

$$G_0^{\nu}(\mathbf{k}, i\omega_n) = \frac{1}{i\omega_n - \varepsilon_{\mathbf{k}}^{\nu}} \tag{1}$$

where $\varepsilon_{\mathbf{k}}^{\nu}$ denotes the ν^{th} DFT band at momentum $\mathbf{k}$. The density fluctuation can be obtained from knowledge of bare Green's function

$$\begin{aligned}
&\chi_0^{\mu\nu}(\mathbf{q}, i\omega_p) \\
&= -\frac{1}{\Omega_{BZ}\beta} \sum_{\mathbf{k},n} G_0^{\mu}(\mathbf{k}, i\omega_n) G_0^{\nu}(\mathbf{k}+\mathbf{q}, i\omega_n + i\omega_p) \qquad (2) \\
&= -\frac{1}{\Omega_{BZ}} \sum_{\mathbf{k}} \frac{f_{\mathbf{k}+\mathbf{q}}^{\mu} - f_{\mathbf{k}}^{\nu}}{i\omega_p + \varepsilon_{\mathbf{k}+\mathbf{q}}^{\mu} - \varepsilon_{\mathbf{k}}^{\nu}} \qquad (3)
\end{aligned}$$

where $\beta = \frac{1}{k_B T}$ with k_B is the Boltzmann constant and T is temperature, Ω_{BZ} is the phase space volume of the Brillouin zone, $\mathbf{q}$ and ω_p are momentum and frequency of the bosonic excitations created by density fluctuations, $f_{\mathbf{k}}^{\nu}$ is the Fermi distribution function for the ν^{th} band. The last equation is obtained by performing Matsubara summation over ω_n. To get the retarded response function $\chi_0^{\mu\nu}(\mathbf{q}, \omega)$ we substitute $i\omega_p \to \omega + i\delta$

$$\chi_0^{\mu\nu}(\mathbf{q}, \omega) = \lim_{\delta \to 0} \chi_0^{\mu\nu}(\mathbf{q}, \omega + i\delta). \tag{4}$$

Next we introduce interaction between bands by interacting Hamiltonian

$$\begin{aligned}
H_{int} = \sum_{\mathbf{k_1},\mathbf{k_2},\mathbf{k_3},\mathbf{k_4}} \Bigg[&\sum_{\nu,\sigma} U^{\nu\nu} c_{\mathbf{k_1}\sigma}^{\nu\dagger} c_{\mathbf{k_2}\sigma}^{\nu} c_{\mathbf{k_3}\bar{\sigma}}^{\nu\dagger} c_{\mathbf{k_4}\bar{\sigma}}^{\nu} \\
&+ \sum_{\nu,(\mu\neq\nu),\sigma,\sigma'} U^{\nu\mu} c_{\mathbf{k_1}\sigma}^{\nu\dagger} c_{\mathbf{k_2}\sigma}^{\nu} c_{\mathbf{k_3}\sigma'}^{\mu\dagger} c_{\mathbf{k_4}\sigma'}^{\mu} \Bigg],
\end{aligned} \tag{5}$$

where $c_{\mathbf{k}\sigma}^{\nu\dagger}(c_{\mathbf{k}\sigma}^{\nu})$ is creation (anihilation) operator for ν^{th} band and momentum $\mathbf{k}$, σ is the spin and $U^{\nu\mu}$ is intraband ($\nu = \mu$) and interband ($\nu \neq \mu$) Coulomb interactions. Interacting many-body density-fluctuation spectrum can be given within RPA approximation as

$$\chi_{c/s}^{\mu\nu}(\mathbf{q}, \omega) = \chi_0^{\mu\nu}(\mathbf{q}, \omega) \left[1 \pm U^{\mu\nu} \chi_0^{\mu\nu}(\mathbf{q}, \omega)\right]^{-1}, \tag{6}$$

where 'c' and 's' stands for charge and spin channel respectively. Next we calculate the density-fluctuation potential with fluctuation-exchange (FLEX) approximation as

$$V_i^{\mu\nu}(\mathbf{q}, \omega) = \frac{\eta_i}{2} \left[U^{\mu\nu} \chi_0^{\mu\nu}(\mathbf{q}, \omega) U^{\mu\nu}\right] \tag{7}$$

where $i = 1$ for spin with $\eta_1 = 3$ and $i = 2$ for charge with $\eta_2 = 1$. Thus the self-energy expression becomes

$$\begin{aligned}
\Sigma_{i,\mu}(\mathbf{k}, \omega) = \frac{1}{\Omega_{BZ}} \sum_{\mathbf{q},\nu} \int_0^{\infty} \frac{d\omega'}{2\pi} V_{i,\mu\nu}(\mathbf{q}, \omega') \Gamma_{\nu}(\mathbf{k}, \mathbf{q}) \\
\left[\frac{1 - f_{\mathbf{k}-\mathbf{q}}^{\nu} + n_p}{\omega + i\delta - \varepsilon_{\mathbf{k}-\mathbf{q}}^{\nu} - \omega_p} + \frac{f_{\mathbf{k}-\mathbf{q}}^{\nu} + n_p}{\omega + i\delta - \varepsilon_{\mathbf{k}-\mathbf{q}}^{\nu} + \omega_p}\right]
\end{aligned} \tag{8}$$

where n_p is the bosonic distribution function for frequency ω_p and $\Gamma(\mathbf{k}, \mathbf{q})$ is the vertex correction included self-consistently. With this self-energy the dressed Green's function can be written as

$$G_{\mu}^{-1}(\mathbf{k}, \omega) = G_{0,\mu}^{-1}(\mathbf{k}, \omega) - \Sigma_{\mu}(\mathbf{k}, \omega) \tag{9}$$

where $\Sigma_{\mu\nu}(\mathbf{k}, \omega) = \Sigma_{1,\mu\nu}(\mathbf{k}, \omega) + \Sigma_{2,\mu\nu}(\mathbf{k}, \omega)$. Now this Green's function(G) can be used to define susceptibility in eq.(3) and the whole process is repeated unless the self-consistency is achieved.

With the self-energy correction a well defined quasiparticle is not possible, except perhaps in the low-energy region where the imaginary part of the self-energy is weak. In this spirit, for the low-energy region we can extract the quasiparticle band as a pole of the Green's function which leads to the self-consistent equation as

$$\bar{\varepsilon}_{\mathbf{k}}^{\nu} = \varepsilon_{\mathbf{k}}^{\nu} + \Sigma_{\nu}'(\mathbf{k}, \bar{\varepsilon}_{\mathbf{k}}^{\nu}), \tag{10}$$

where $\varepsilon^{\nu}_{\mathbf{k}}$ is the DFT band and $\bar{\varepsilon}^{\nu}_{\mathbf{k}}$ is the self-energy corrected band. We compare these two results for NNO/STO and NNO/YAO samples in Fig. S5. We find that quasiparticle bands (red dots) are renormalized compared to the non-interacting bands (black dots) throughout the BZ. Expectedly the quasiparticle bands are well defined in the low-energy region, while at higher-energy it fails to maintain a one-to-one correspondence with the non-interacting bands due to multi-band effects.

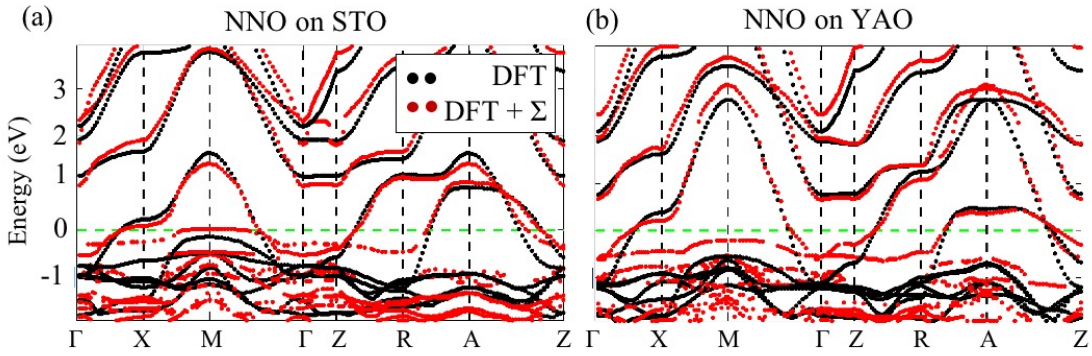

FIG. S5. (a)-(b) Computed band structure for the two representative samples. Blue and red dots represent the result without and with self-energy corrections, as discussed in the text.

Relation between pseudocubic and tetragonal Brillouin zone

As explained in main text, the characteristic E' antiferromagnetic wave vector for $RE\mathrm{NiO}_3$ is (1/4, 1/4, 1/4) in pseudocubic setting [6]. The same magnetic wave vector will be around the (1/4, 1/4, 1/2) in reciprocal space of the tetragonal unit cell (used for calculation in this paper). In order to check the issue of nesting around this (1/4, 1/4, 1/2) point, RPA spin susceptibility has been calculated along ZA (Fig. S6(d)).

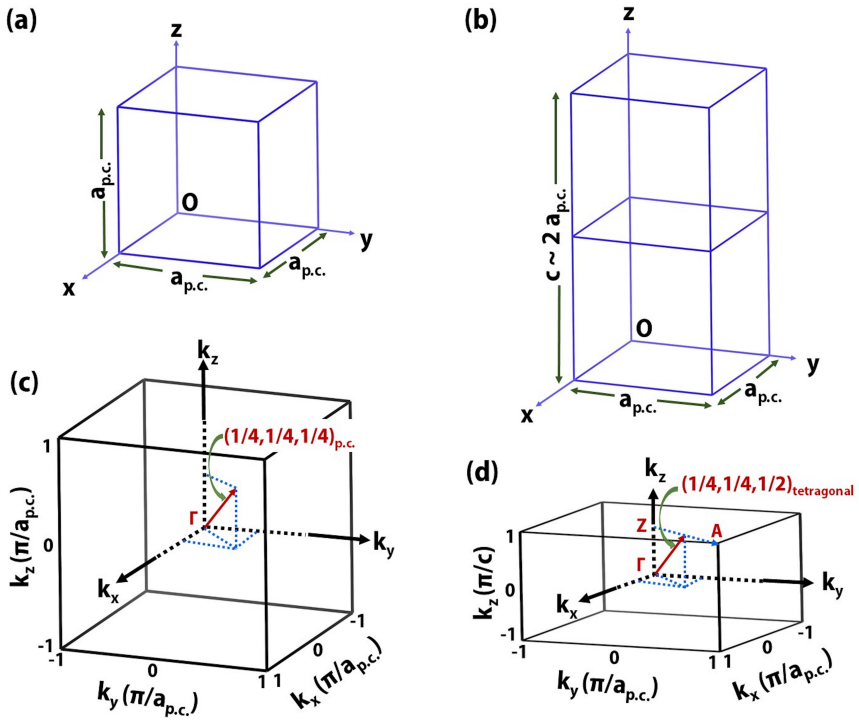

FIG. S6. Unit cell in (a) pseudocubic and (b) tetragonal settings. As explained in the main text, this tetragonal unit cell has been used for DFT calculation. Corresponding Brillouin zone for cubic and tetragonal unit cell, along with the E'-AFM wave vector has been plotted in (c) and (d), respectively.

Calculation of RPA spin susceptibility

In Fig. S7, we have plotted the real-part of the RPA spin susceptibility along ZA. As demonstrated earlier [7–9], we find a strong nesting peak near $\mathbf{q} = (1/4, 1/4, 1/4)$ (in-pseudocubic notation) [$\equiv$ (1/4, 1/4, 1/2) in tetragonal setting] in the NNO/STO system, while the peak is substantially weak in the case of NNO/YAO. The strong peak in susceptibility localized at a preferential wave vector indicates the presence of spin-density wave (SDW) instability. Based on these results, we conclude that NNO/STO is more susceptible to form a SDW state than the NNO/YAO sample which is consistent with the experimental trends of antiferromagnetic to nonmagnetic state in going from NNO/STO to NNO/YAO samples.

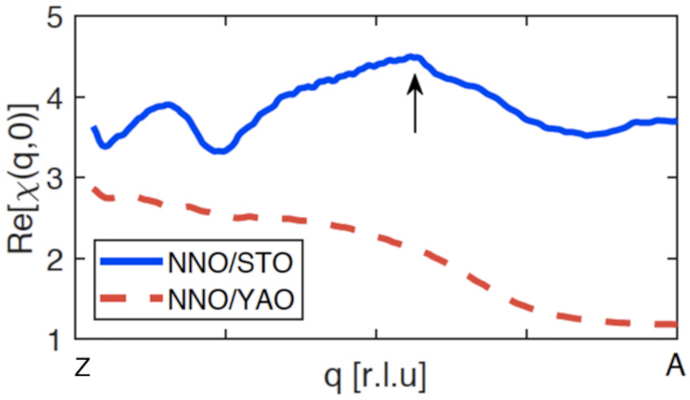

FIG. S7. Computed static spin susceptibility within RPA model for NNO on STO and NNO on YAO.

[1] S. D. Ha, R. Jaramillo, D. M. Silevitch, F. Schoofs, K. Kerman, J. D. Baniecki, and S. Ramanathan, Phys. Rev. B **87**, 125150 (2013).
[2] T. Das, J.-X. Zhu, and M. J. Graf, Phys. Rev. Lett. **108**, 017001 (2012).
[3] T. Das and K. Dolui, Phys. Rev. B **91**, 094510 (2015).
[4] T. Das, R. Markiewicz, and A. Bansil, Advances in Physics **63**, 151 (2014), https://doi.org/10.1080/00018732.2014.940227.
[5] R. S. Dhaka, T. Das, N. C. Plumb, Z. Ristic, W. Kong, C. E. Matt, N. Xu, K. Dolui, E. Razzoli, M. Medarde, L. Patthey, M. Shi, M. Radović, and J. Mesot, Phys. Rev. B **92**, 035127 (2015).
[6] S. Middey, J. Chakhalian, P. Mahadevan, J. W. Freeland, A. J. Millis, and D. D. Sarma, Annual Review of Materials Research **46**, 305 (2016).
[7] S. Lee, R. Chen, and L. Balents, Phys. Rev. Lett. **106**, 016405 (2011).
[8] S. Lee, R. Chen, and L. Balents, Phys. Rev. B **84**, 165119 (2011).
[9] H. K. Yoo, S. I. Hyun, L. Moreschini, H.-D. Kim, Y. J. Chang, C. H. Sohn, D. W. Jeong, S. Sinn, Y. S. Kim, A. Bostwick, E. Rotenberg, J. H. Shim, and T. W. Noh, Sci. Rep. **5**, 8746 (2015).